





Article

Bacterial toxicity of sulfidated nanoscale zerovalent iron in aerobic and anaerobic systems: implications for chlorinated solvent clean-up strategies

Adrian A. Schiefler^{1,2} , Nina Tuxen², Sathish Mayanna^{3,4}, Liane G. Benning^{3,5}  and Dominique J. Tobler⁶

¹Department of Physics, Technical University of Denmark, Fysikvej, 2800 Kongens Lyngby, Denmark; ²Groundwater Section, Capital Region of Denmark, 3400 Hillerød, Denmark; ³GFZ German Research Center for Geosciences, Telegrafenberg, 14473 Potsdam, Germany; ⁴Carl Zeiss Microscopy GmbH, Carl Zeiss Strasse 22, 73447, Oberkochen, Germany; ⁵Department of Earth Sciences, Free University of Berlin, 12249 Berlin, Germany and ⁶Department of Plant and Environmental Sciences, University of Copenhagen, Thorvaldsensvej 40, 1871 Frederiksberg C, Denmark

Abstract

Sulfidated nanoscale zerovalent iron (S-nZVI) materials show enhanced reactivity and selectivity towards chlorinated solvents compared to non-sulfidated nZVI, thus they have a high potential for subsurface chlorinated solvent remediation. However, little is known about the possible toxic effects of S-nZVI towards microbial communities, which is of particular concern with regard to combined abiotic–biotic chlorinated solvent treatment scenarios. In this study, the toxicity of two different S-nZVI materials towards *Shewanella oneidensis* MR-1 (S. MR-1) was examined under anaerobic and aerobic conditions using colony forming units (CFU) and adenosine triphosphate (ATP) measurements, and the results were then compared to identical exposures performed with non-sulfidated nZVI. In a second step, the toxicity of S-nZVI and nZVI materials was tested on the commercial bioremediation culture KB-1* and on an in-house trichloroethylene enrichment culture. Under aerobic conditions, S. MR-1 viability was less affected by S-nZVI materials compared to non-sulfidated nZVI materials (up to three times higher viability) and it was generally lower compared to anaerobic conditions where little difference in S. MR-1 viability was observed between the tested materials. In terms of the two dechlorinating cultures, they exhibited significantly higher ATP viability during anaerobic exposures to S-nZVI and nZVI materials. Particularly for KB-1*, which retained comparable ATP-viability after ~60 hours exposure as S. MR-1 after two hours. Moreover, the ATP viability of the mixed cultures was generally higher in S-nZVI exposures compared to nZVI exposures (up to three times higher viability). The observed viability patterns are explained by differences in the shell structure, chemistry and stability of the tested S-nZVI and nZVI materials towards corrosion, while the substantially enhanced resilience of KB-1* is argued to stem from its year-long cultivation in the presence of reduced FeS particulates.

Keywords: nanoparticle toxicity; combined biotic/abiotic remediation; ATP; KB-1*; *Shewanella oneidensis* MR-1; S-nZVI

(Received 03 January 2024; revised 24 March 2024; manuscript accepted: 03 April 2024)

Highlights

- Sulfidation of nZVI with Na₂S reduces bacterial toxicity under aerobic conditions
- Differences between CFU and ATP-based viabilities show differences in inactivation mechanisms originating from different particle shell structures
- Sulfidation of nZVI reduces inactivation of KB-1* culture
- KB-1* shows high resilience to (S-)nZVI exposure, compared to an in-house culture

Corresponding authors: Adrian Schiefler and Dominique Tobler; Emails: aalsc@dtu.dk; dominique.tobler@plen.ku.dk

Cite this article: Schiefler A.A., Tuxen N., Mayanna S., Benning L.G., & Tobler D.J. (2024). Bacterial toxicity of sulfidated nanoscale zerovalent iron in aerobic and anaerobic systems: implications for chlorinated solvent clean-up strategies. *Geo-Bio Interfaces* 1, e2, 1–10. <https://doi.org/10.1180/gbi.2024.1>

Introduction

The past uncontrolled release of chlorinated solvents, particularly perchloro- and trichloro-ethylene (PCE, TCE), has led to chlorinated solvent contaminated soils and aquifers worldwide that pose significant threats to groundwater security. In saturated soils, chlorinated hydrocarbon compounds are degraded via microbial reductive processes but the rates are relatively low and degradation often stops at more toxic intermediate products. Microbial reductive dechlorination can be stimulated either by injection of organic substrates (Atashgahi *et al.* 2018) or, if native dechlorinating species are absent and/or incapable of full dechlorination, by the injection of a dechlorinating culture such as KB-1* (Duhamel *et al.* 2002). Much higher rates of chlorinated solvent degradation can be achieved by the injection of micro and nanoscale zero-valent iron (m/nZVI) materials, but compared to microbial dechlorination this abiotic approach has limited longevity due to fast Fe⁰ corrosion by non-target solutes, as well as a limited radius of influence due to

limited ZVI mobility upon injection. As a result, combined ZVI-biotic treatment scenarios have become increasingly popular as one technique can complement the shortcomings of the other. For example, in the case of nZVI, the hydrogen produced by anaerobic corrosion can help stimulate microbial dechlorination by supplying electrons to hydrogenotrophic bacteria, and Fe⁰ corrosion itself can create a suitable reducing environment for the growth of anaerobic bacteria needed in this process (Dong *et al.* 2019).

More often, however, the highly reactive nature of ZVI, particularly nZVI, has been shown to have harmful effects on microbial viability (Lefevre *et al.* 2015; Semerád and Cajthaml 2016) and microbial dechlorination. Studies have reported a decrease in dechlorination rates at nZVI concentrations as low as 50 mg/L (Xiu *et al.* 2010b; Velimirovic *et al.* 2015; Kocur *et al.* 2015, 2016; Rónavári *et al.* 2016). In several cases (Velimirovic *et al.* 2015; Kocur *et al.* 2016), microbial dechlorination rates increased again after extended lag phases, indicating that these cultures could grow again after initial impairment. In general, nZVI toxicity is reported to be highest under anaerobic conditions (Lee *et al.* 2008; Kim *et al.* 2010; Li *et al.* 2010), where nZVI exhibits highest reactivity with chlorinated solvents. The toxicity is argued to arise via cell/membrane disruption due to direct cell-particle interactions (Li *et al.* 2010; Xiu *et al.* 2010b; Chen *et al.* 2011; Zhou *et al.* 2014; Dong *et al.* 2016), oxidative stress induced by the Fe²⁺ produced during anaerobic nZVI corrosion (Lee *et al.* 2008) and cell encapsulation by iron corrosion products (Diao and Yao 2009). Under aerobic conditions, where nZVI toxicity seems lower, the above-mentioned toxicity pathways certainly apply but the main, or maybe fastest, acting toxicity pathway is attributed to oxidative stress via the formation of reactive oxygen species (ROS) by chemical activation of dissolved oxygen (Wu *et al.* 2014; Lefevre *et al.* 2015; Semerád and Cajthaml 2016).

Over the past 10 years, sulfidation of nZVI (S-nZVI) has emerged as a new strategy to protect the Fe⁰ core from fast corrosion while increasing its selectivity and reactivity towards pollutants such as chlorinated solvents and ensuring enhanced longevity once injected (Kim *et al.* 2011; Fan *et al.* 2013, 2016, 2017; Tang *et al.* 2016; Xu *et al.* 2016; Song *et al.* 2017; Wu *et al.* 2018; Mangayayam *et al.* 2019b; Garcia *et al.* 2021). It has recently been shown that sulfidation could lower nZVI toxicity towards microbial cells (Garcia *et al.* 2021). For example, both Cheng *et al.* (2019a) and Han *et al.* (2019) showed that an increase in nZVI sulfidation led to a decrease in toxicity towards *Escherichia coli* under anaerobic conditions. Both name physical cell membrane disruption or penetration as the main inactivation pathway while Cheng *et al.* identified ROS as the main mediator of toxicity, which in turn suggests that the conditions employed by Cheng *et al.* were at least partially aerobic. Semerád *et al.* (2020) investigated S-nZVI toxicity under aerobic conditions and showed that the oxidative stress in *Pseudomonas putida* decreased with increasing nZVI sulfidation. Overall, these three studies indicate that sulfidation of nZVI lowers toxicity towards microbial cells. However, only two bacterial strains were tested using different sulfidation protocols, S-nZVI materials and different experimental conditions (for example, particle loadings of 10 mg/l vs 500 mg/l), making comparison and interpretation of toxicity pathways difficult. In addition, given the increased interest in combined abiotic–biotic remediation treatment scenarios, it is critical that the toxicity of sulfidated nZVI is also assessed on dechlorinating cultures, which is absent from the literature thus far.

In this study, *Shewanella oneidensis* MR-1, a facultative anaerobic metal reducer, was exposed to two different S-nZVI materials and to nZVI (at 100 mg/L particle loadings) under both aerobic and

anaerobic conditions to assess their toxicity. Toxicity was measured after 20, 60 and 120 minutes by measuring cell viability via two assays: classical colony forming units (CFU) and the adenosine triphosphate (ATP) bioluminescence method. The CFU method provides a measure of viable clonogenic cell numbers while the ATP method provides a fast and instantaneous measure of overall metabolic cellular viability and can be applied to all bacterial strains (or mixtures thereof); thus, it overcomes some disadvantages of other methods (for example, CFU limited to easily culturable strain(s), and DNA and qPCR analyses using costly, specialized equipment). In a second step, the toxicity of S-nZVI and nZVI materials was also assessed on mixed dechlorinating bacterial communities, as would be relevant in combined abiotic/biotic chlorinated solvent remediation treatment. Here, the ATP viability of the commercial bioremediation culture KB-1[®] and an in-house TCE degrading enrichment culture was monitored upon exposure to S-nZVI and nZVI materials over one week. In these experiments, particle loading was increased to 1000 mg/l, which is representative of conditions during field scale remediation treatment. The implications of the study results for combined abiotic/biotic treatment scenarios are discussed below.

Methods

All solutions were prepared using reagent grade chemicals and deionized MilliQ-water (DI, resistivity = 18.2 Ωcm). All material syntheses and anaerobic toxicity studies with *S. oneidensis* MR-1 were performed inside an anaerobic vinyl glove box (97% N₂/3% H₂; Coy laboratories), and all work related to the mixed cultures was performed in a hard-walled anaerobic chamber with catalytic oxygen removal (MBraun, O₂ levels < 0.1 ppm) that was regularly sterilized using UV-C radiation. For anaerobic procedures, DI water was deoxygenated by first sparging with N₂ for at least 30 minutes and then equilibrated inside the anaerobic glove box overnight (abbreviated as DO/DI henceforth).

Material synthesis and characterization

Nanoscale ZVI (nZVI) was synthesized by first mixing 50.1 ml of 0.35 mM FeCl₂·4H₂O with 21.5 ml of 96% ethanol. Next, 35.8 ml of 1.48 mM NaBH₄ were titrated to the Fe²⁺-ethanol mixture at a flow rate of 5 ml/min under constant stirring (He and Zhao 2007; Sun *et al.* 2006). The suspension was then stirred for another eight minutes, followed by the collection of nZVI materials using a strong magnet. Two different S-nZVI materials were synthesized by using either sodium sulphide or sodium dithionite in the sulfidation step. For this, nZVI materials were resuspended in 120 ml of 0.2 M acetate buffer (pH 5.6), sonicated for 15 minutes, then 4.2 ml of either 1 M Na₂S or 0.5 M Na₂S₂O₄ were added (S/Fe = 0.24) to create Na₂S-nZVI and Na₂S₂O₄-nZVI materials, respectively. The suspensions were sonicated for another five minutes and then placed on a shaker for three hours. Materials were collected by a magnet and briefly rinsed twice with DO/DI and once with O₂-free methanol (10 ml each) before drying overnight in a vacuum at 25°C. The dried materials were then gently ground into powder. Fresh materials were prepared every two weeks.

Freshly synthesized nZVI and S-nZVI materials were characterized using transmission electron microscopy (TEM), X-ray photoelectron spectroscopy (XPS) and high-resolution X-ray scattering to determine potential differences in the core-shell architecture between these materials. TEM samples were prepared by

drop-casting 3 μ l of material suspension (in ethanol) on formvar-coated copper TEM grids and then analysed on a Philips CM20 at an accelerating voltage of 200 kV. For XPS, dry material was packed on XPS aluminium stubs inside the anaerobic chamber, and a drop of methanol was added to wet the samples. The stubs were transferred to the XPS (Kratos Axis Ultra^{DLD} with a monochromatic Al K α X-ray source, $h\nu = 1486.6$ eV, power = 150 W) using an anaerobic XPS holder and analysed using a pass energy of 20 eV. XPS spectral analyses were performed in CasaXPS following previous procedures (Mangayayam 2019a). High energy X-ray diffraction was performed at beamline 11-ID-B at the Advanced Photon Source, Argonne National Laboratories, USA (58 kV, $\lambda = 0.2114$ Å) using a 40×40 cm amorphous Si 2D detector placed at a sample-to-detector distance of 18 cm for pair distribution function analysis (PDF) and 100 cm for X-ray diffraction. Dried powder samples were inserted into glass capillaries and sealed with paraffin wax under inert atmospheric conditions, according to previously established procedures (Mangayayam 2019a). More details on sample analysis and spectra handling are provided in the supplementary file (Text S4). Lastly, the material-cell association in *S. MR-1* anaerobic exposures (explained below) was probed using field emission scanning electron microscopy (Zeiss Ultra Plus FESEM, 3–5 kV). For this, material-cell pellets (as obtained from centrifugation) were fixed with 2.5% glutaraldehyde overnight and then dehydrated using ethanol. Samples were coated with a ~20 nm-thick layer of carbon using a sputter coater.

Bacterial cultures

Shewanella oneidensis MR-1 (*S. MR-1*; ATCC® 700550™) was grown aerobically on lysogeny broth (LB) agar plates from frozen stocks. For experiments, 50 ml sterile LB were inoculated with *S. MR-1* from agar plates and incubated for ~18 h at 30°C, under shaking (110 rpm) until the cells reached the end of the exponential growth phase. Cell suspensions were pelleted by centrifugation (5 min, 2800xg) and washed twice with a 0.85 wt.% NaCl solution before resuspending to an optical density (OD_{600nm}) of 0.31–0.32 (~ 3×10^8 cells/ml). For anaerobic experiments, cells were washed and OD₆₀₀ adjusted inside the anaerobic chamber using a 0.85 wt.% NaCl solution prepared with DO/DI. All bacterial suspensions were used immediately for viability testing.

The bioremediation culture KB-1* was obtained from SiREM (Guelph, Canada), where it had been cultivated under the same conditions for many years (Duhamel *et al.* 2002; Pérez-de-Mora *et al.* 2018). It was received as an anaerobic suspension, stored at 4°C and used within two weeks of receipt. Prior to removing a suspension sample for viability testing, the headspace was purged with sterile N₂ to remove residual electron acceptors.

The in-house enrichment culture was started by inoculating 50 ml of sterile, reduced synthetic mineral medium (Löffler *et al.* 2005) with 50 ml of chlorinated solvent-contaminated groundwater from well B111 of the Innovation Garage site, Skovlunde (Sjælland, Denmark) that had previously been shown to contain dechlorinating species, including *Dehalococcoides* and *Dehalogenimonas* and low levels of *vcr* reductase (that is, functional genes encoding for vinyl chloride degradation) (Schiefler *et al.* 2018). The medium contained TCE as an electron acceptor and lactate and methanol as an electron donor and carbon source, respectively. More details on culture medium preparations are given in the Supplementary materials (Text S1). The culture was enriched by repeatedly transferring 10% of the grown culture to a fresh medium for almost a year (Figure S1). To prepare the enriched culture for toxicity assays,

10% of the grown culture were transferred to a fresh medium and amended with three successive cycles of donor/acceptor (while replacing 10% with fresh medium) to reach a viability close to KB-1*, according to ATP measurements. The headspace was purged before use, as for KB-1*.

Experimental setup for viability testing

Triplicate *S. MR-1* exposures were performed on different days using a newly grown culture, while triplicate mixed culture exposures were performed on the same day using the same culture. For each experiment, dry nZVI and S-nZVI materials were first resuspended in DO/DI (at 10 g/l) inside crimp-capped vials, sonicated for five minutes and then diluted once more depending on final material loading (that is, 100, 500 or 1000 mg/l). Exposure experiments were set up in 2 ml centrifuge tubes by mixing 0.1 ml of the prepared material stocks with 0.9 ml bacterial suspension. Bacterial controls were amended with DO/DI instead of nZVI/S-nZVI materials. All tubes were placed on an orbital shaker and sacrificially sampled after 0.3, 1 and 2 hours for *S. MR-1* exposures, while the mixed culture exposure experiments were regularly monitored for up to 156 hours. Anaerobic experiments were conducted inside the anaerobic glove box while aerobic experiments were performed outside on the lab bench, both at ambient temperatures.

Cell viability assays

Plate counting: The method was adapted from the single plate-serial dilution spotting (SP-SDS) method (Thomas *et al.* 2015). In short, 9 sectors were drawn on LB agar plates and 20 μ l aliquots from 3 relevant dilutions (prepared in phosphate buffer saline) were spotted (in triplicate) as 10–12 micro-droplets in each sector. The number of viable cells was derived by counting the colony-forming units (CFU) on each plate which were then averaged across triplicates.

ATP bioluminescent assay: ATP tests were performed with BacTiter-Glo (Promega) as per the manufacturer's recommendations and bioluminescence was measured by a Fluoroskan ascent FL (ThermoSci). Due to the dark colour of the S-nZVI and nZVI materials, which quenches luminescent signals (false negatives), some additional amendments were necessary. In viability tests with *S. MR-1*, this false negative impact could be minimized by serial dilution because of the low material loading (100 mg/L) and the large detectable ATP range (details in Text S2, Figs S2 and S3). In viability tests with the two mixed cultures, where a higher material loading was applied (that is, 500 and 1000 mg/L), serial dilution did not work. Instead, the ATP reagent was added directly to exposures to induce cell lysis before separating the materials by centrifugation and analysing the supernatant (details in Text S3).

ATP and CFU viabilities (%) in exposures were derived with respect to ATP and CFU values determined in bacterial controls (with no added materials). Furthermore, the difference between the two viability measures, $\Delta_{\text{Assay}} = \text{ATP-viability} - \text{CFU-viability}$, was determined to test for any systematic variations in cell impairment/toxicity mechanisms between the different materials. Such differences may arise because ATP can still be retained by cells that cannot reproduce under CFU test conditions. For example, CFU inactivation by starvation, impairment and growth inhibition or a form of necrosis (Chappelle *et al.* 1978; Oliver 2005, 2010; Pan and Ren 2023) is also described as a viable but non-culturable state (VBNC) (Beumer *et al.* 1992; Federighi *et al.* 1998; van Tatenhove-Pel *et al.* 2019). Entering such a vegetative state, which allows cells to endure stress and adverse conditions, seems to depend on strain

and stressor (Su *et al.* 2015) and thus could vary between tested materials. As an example, if the measured ATP-viability remains high with increasing exposure to nZVI/S-nZVI, while the measured CFU-viability decreases, reflected by Δ_{Assay} values increasing with exposure time, this could be reflective of an increase in VBNC cell numbers. By contrast, if cell impairment by nZVI/S-nZVI materials leads directly to cell death, then it is expected that ATP and CFU viabilities decrease proportionally, reflected by fairly constant Δ_{Assay} values with exposure time.

Results and discussion

Initial material characterization

Transmission electron microscopy images of nZVI (Fig. 1a) and nZVI sulfidated with sodium sulfide (Na_2S -nZVI, Fig. 1b) showed well-defined, spherical particles with diameters of around 50 to 150 nm, while nZVI sulfidated with sodium dithionite ($\text{Na}_2\text{S}_2\text{O}_4$ -nZVI, Fig. 1c) exhibited similar sized, spherical particles that were also surrounded by thin, sheet-like structures (Fig. 1c). Taking a closer look, Na_2S -nZVI particles exhibited a thin shell of lower contrast, generally less than 10 nm in thickness (inset in Figure 1b), which was less defined for $\text{Na}_2\text{S}_2\text{O}_4$ -nZVI due to the surrounding sheet-like structures and totally absent in nZVI materials (inset in Fig. 1a). Overall, these observations match high-resolution TEM characterizations performed on identical nZVI and S-nZVI materials (fig. 2 in Mangayayam *et al.* 2019b, fig. S1 in Mangayayam *et al.* 2019a).

X-ray photoelectron spectroscopy confirmed differences in particle shell structure in the three materials, as indicated by TEM images. Specifically, XPS data showed the presence of a sulfur species on Na_2S -nZVI and $\text{Na}_2\text{S}_2\text{O}_4$ -nZVI particle surfaces, which were absent on nZVI particles (Table S1 and Fig. S4). Sulfide (S^{2-}) was the most dominant sulfur species in both sulfidated nZVI particles (~80% of detected sulfur), while other sulfur species (for example, S_2^{2-} , S_n^{2-}) constituted only minor phases (~20%, Table S2). High-resolution XPS scans for Fe 2p (Fig. S4) revealed that relative to $\text{Na}_2\text{S}_2\text{O}_4$ -nZVI, nZVI and Na_2S -nZVI materials exhibited a higher abundance of reduced iron species (Fe^0 , Fe^{2+} -S, Table S2). Conversely, $\text{Na}_2\text{S}_2\text{O}_4$ -nZVI exhibited larger Fe surface and Fe^{2+} satellite peaks, which are indicative of high-spin Fe coordination, as observed in Fe (hydr)oxides (Grosvenor *et al.* 2004; Mullet *et al.* 2008). This suggested that $\text{Na}_2\text{S}_2\text{O}_4$ -nZVI materials contained a higher amount of oxidized Fe species compared to nZVI and Na_2S -nZVI. Overall, oxygen was the

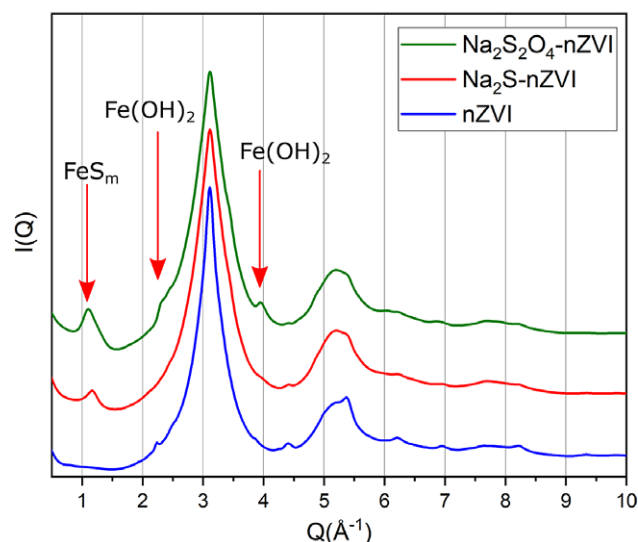


Figure 2. HEXRD patterns of nZVI, Na_2S -nZVI and $\text{Na}_2\text{S}_2\text{O}_4$ -nZVI. Reflections are annotated as Fe^0 for the nZVI core, FeS_m and Fe(OH)_2 for mackinawite and ferrous hydroxide present in the S-nZVI shell.

dominant surface species in all three materials, which was also observed in previous studies on these materials (Kim *et al.* 2011; Song *et al.* 2017; Su *et al.* 2019). The O 1s XPS spectra (Fig. S4) further confirmed that material surfaces were a little oxidized as shown by the presence of O^{2-} species.

High energy X-ray scattering data confirmed that nZVI and sulfidated nZVI materials mainly consisted of nanocrystalline metallic iron as identified by the broad peaks at Q values of 3.09 and 5.35 \AA^{-1} (Fig. 2) (Wyckoff 1963). The sulfidated nZVI materials, Na_2S -nZVI and $\text{Na}_2\text{S}_2\text{O}_4$ -nZVI, showed an additional peak at $1.1\text{--}1.2 \text{ \AA}^{-1}$, which matches mackinawite (FeS_m) with an expanded basal plane spacing, as observed previously for these materials (Fan *et al.* 2013; Mangayayam *et al.* 2019b). Lastly, some smaller peaks and shoulders were observed for $\text{Na}_2\text{S}_2\text{O}_4$ -nZVI at Q values of ~1.3, 2.3 and 4 \AA^{-1} , which fit reasonably well with the characteristic peaks of Fe(OH)_2 (Fig. 2) (Mangayayam *et al.* 2019a). Fe(OH)_2 often forms sheet-like, flaky particles, so this fits well with the sheet-like structures observed for $\text{Na}_2\text{S}_2\text{O}_4$ -nZVI in TEM images (Fig. 1c). A previous study on one-pot sulfidated nZVI with $\text{Na}_2\text{S}_2\text{O}_4$ also

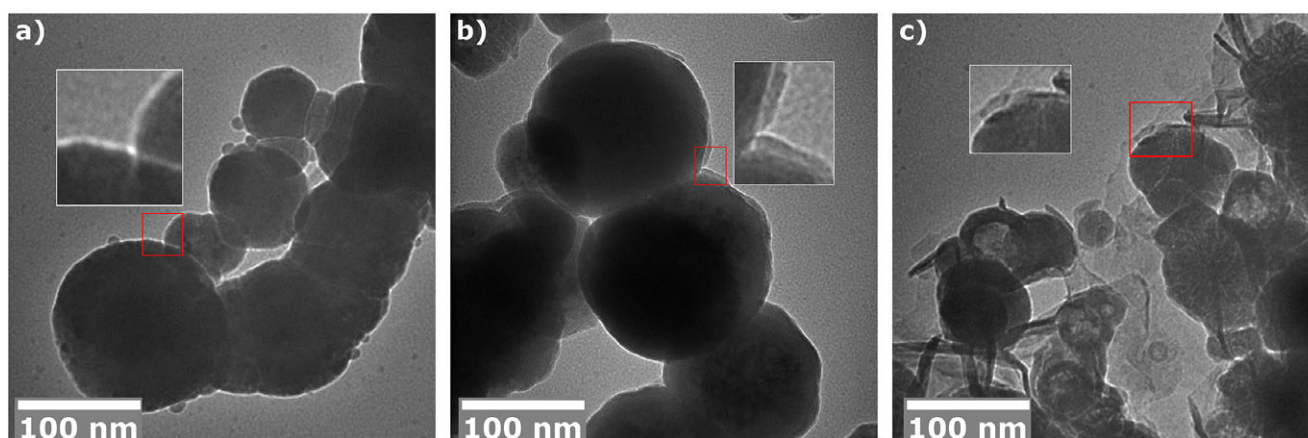


Figure 1. TEM images of freshly synthesized materials showing the differences in core-shell morphology: (a) nZVI particles with no apparent shell; (b) Na_2S -nZVI particles with lower density shell; (c) $\text{Na}_2\text{S}_2\text{O}_4$ -nZVI particles with diffuse shells and surrounded by flaky structures. Insets show a close-up of particle shell regions.

observed $\text{Fe}(\text{OH})_2$ in the particle shell, which the authors confirmed by looking at the PDF of these materials. This was also done here (details in the Supplementary materials), with the results shown in Fig. S5. These analyses reaffirmed the presence of FeS_m in both sulfidated materials and the additional presence of $\text{Fe}(\text{OH})_2$ on the surfaces of $\text{Na}_2\text{S}_2\text{O}_4$ -nZVI.

In summary, nZVI materials consisted of spherical, nanocrystalline metallic iron particles with a slightly oxidized surface as expected for these materials from previous reports (Han *et al.* 2015; Nurmi *et al.* 2011; Sun *et al.* 2006). Na_2S -nZVI materials resembled nZVI particles in size and shape but exhibited a thin iron sulfide layer that resembled mackinawite, matching previous studies on similarly synthesized Na_2S -nZVI materials (Mangayayam *et al.* 2019a, 2019b; Xu *et al.* 2019). $\text{Na}_2\text{S}_2\text{O}_4$ -nZVI materials also exhibited a mackinawite-like phase in their shell structure but the particles were further surrounded by larger, sheet-like structures that were identified as $\text{Fe}(\text{OH})_2$. Overall, $\text{Na}_2\text{S}_2\text{O}_4$ -nZVI seemed to exhibit the most heterogeneous surface composition in terms of Fe and S phases.

Shewanella oneidensis MR-1 exposure to nZVI and S-nZVI materials

Viability under aerobic vs anaerobic conditions

The viability of *S. MR-1* cells in aerobic exposures to nZVI, Na_2S -nZVI and $\text{Na}_2\text{S}_2\text{O}_4$ -nZVI materials, as probed by CFU and ATP assays, is shown in Figs 3a and 3b, respectively. Qualitatively, CFU and ATP cell viabilities followed similar trends over the 120-minute exposure, showing an initial fast decrease in *S. MR-1* cell viability (ATP: 50–70%; CFU: 60–90%) within the first 20 minutes, which was then followed by a considerably slower decrease. Moreover, both assays showed that cell viabilities were lowest in nZVI and highest in

Na_2S -nZVI exposures, while in $\text{Na}_2\text{S}_2\text{O}_4$ -nZVI exposures, CFU cell viabilities were as low as in nZVI exposures but ATP cell viabilities were in-between those trends observed for Na_2S -nZVI and nZVI.

Under anaerobic conditions, the decrease in *S. MR-1* cell viability upon exposure to nZVI, Na_2S -nZVI and $\text{Na}_2\text{S}_2\text{O}_4$ -nZVI (Figs 3d, 3e) was considerably slower than under aerobic conditions (Figs 3a, 3b), particularly within the first hour. In fact, little change in ATP cell viability occurred between 20- and 60-minute exposures. The largest decrease in cell viability occurred between 60- and 120-minute exposures, reaching similarly low values as under aerobic exposures, particularly when looking at the CFU data (Table S3). ATP cell viabilities after 120 minutes were generally still higher under anaerobic conditions when compared to aerobic conditions. This suggests that ultimate cell death was, overall, less rapid under anaerobic conditions. Noteworthy, if monitored for longer time periods, ATP viabilities in anaerobic exposures would have likely decreased further. In contrast to observations under aerobic conditions, little differences in *S. MR-1* viability time trends were observed between the three materials under anaerobic conditions (usually within one standard deviation of one another).

Independent of exposure conditions, ATP viabilities were typically higher than CFU viabilities (Fig. 3) and this viability difference ($\Delta_{\text{Assay}} = \% \text{ATP} - \% \text{CFU}$) likely reflects some degree of cell impairment that leads to viable but non-culturable cells (VBNC); that is, cells that can still retain/produce ATP but are non-culturable under the employed CFU assay (as described in section 2.5). In Figs 3c and 3f, Δ_{Assay} is plotted for each sampling time for aerobic and anaerobic exposures, respectively. Under aerobic conditions, Δ_{Assay} decreased with time in exposures to nZVI and $\text{Na}_2\text{S}_2\text{O}_4$ -nZVI, suggesting the relative number of VBNC cells decreased with time; that is, cell death became more dominant. By contrast, Δ_{Assay} steadily increased in exposures to Na_2S -nZVI (Fig. 3c), suggesting the relative amount of VBNC cells increased. Contrarily, under

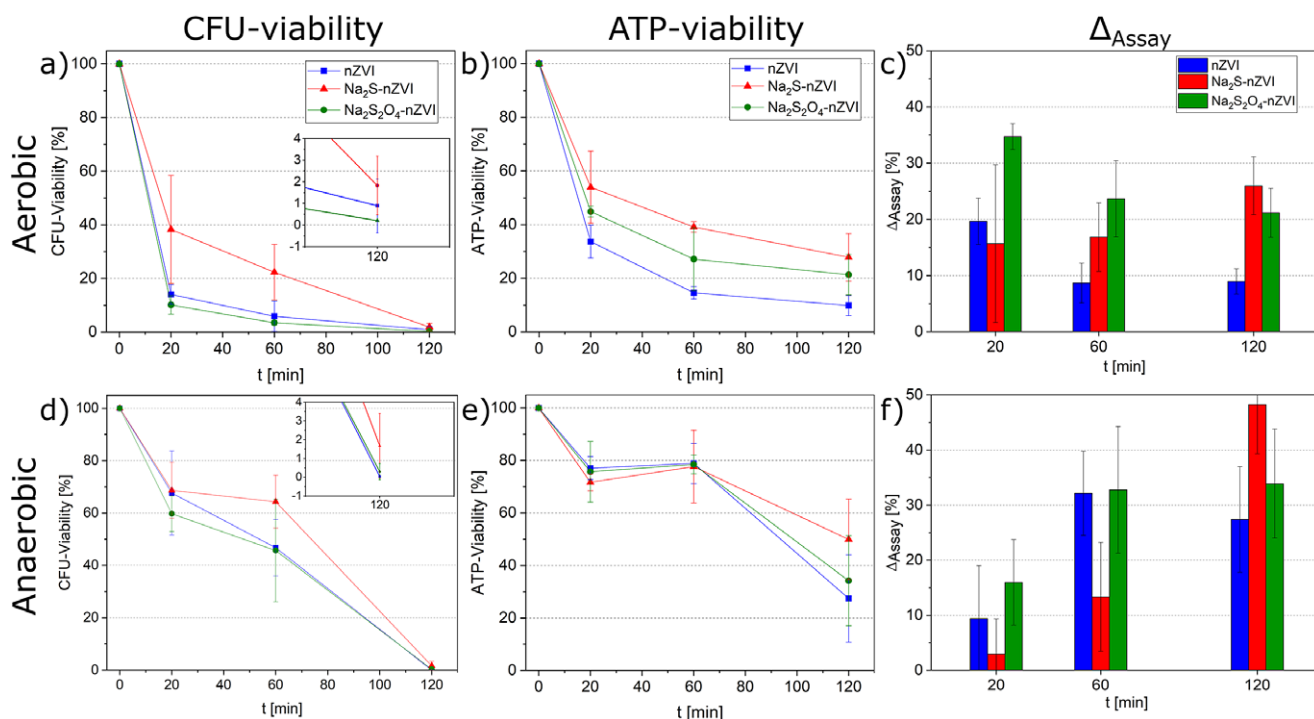


Figure 3. Viability of *Shewanella oneidensis* MR-1 upon exposure to 100 mg/L nZVI, Na_2S -nZVI and $\text{Na}_2\text{S}_2\text{O}_4$ -nZVI under (a–c) aerobic and (d–f) anaerobic conditions: (a, d) CFU-viability, (b, e) ATP-viability and (c, f) Δ_{Assay} ($\% \text{ATP} - \% \text{CFU}$). The plotted data represent the average of triplicate experiments conducted on different days, with errors showing one standard deviation (see Supplementary information eq 2).

anaerobic exposures, Δ_{Assay} increased with time in all material exposures (that is, an increase in VBNC cells relative to cell death); however, much more in $\text{Na}_2\text{S-nZVI}$ exposures (exponential trend from a low level) compared to nZVI and $\text{Na}_2\text{S}_2\text{O}_4\text{-nZVI}$ trends (level off, asymptotic trend). Thus, also under anaerobic conditions, Δ_{Assay} trends in nZVI and $\text{Na}_2\text{S}_2\text{O}_4\text{-nZVI}$ exposures seemed more similar to each other rather than what was observed for $\text{Na}_2\text{S-nZVI}$.

Given that *S. MR-1* viability experiments were all performed in the same way, with triplicates performed on different days using fresh cultures, it seems that the different ATP/CFU viabilities and Δ_{Assay} trends observed for $\text{Na}_2\text{S-nZVI}$ compared to nZVI and $\text{Na}_2\text{S}_2\text{O}_4\text{-nZVI}$ could be due to different impairment mechanisms acting in the respective systems. This may not be surprising, given these materials exhibited different particle shell structures and chemistries as described above (in section on Initial material characterization). Specifically, it was shown that $\text{Na}_2\text{S-nZVI}$ particle surfaces were dominated largely by FeS_m while nZVI and $\text{Na}_2\text{S}_2\text{O}_4\text{-nZVI}$ particle surfaces were more dominated by Fe (hydr)oxide phases. While not measured directly here, it is known that FeS_m surfaces are more hydrophobic and have a lower point of zero charge than Fe (hydr)oxide phases such as $\text{Fe}(\text{OH})_2$ and magnetite (Bhattacharjee and Ghoshal 2018b, 2018a; Xu *et al.* 2020). In turn, this would affect ROS chemistry and physicochemical interactions with bacterial cells (Li *et al.* 2010), thus material toxicity.

Indications for impairment mechanisms

Under aerobic conditions, cell viability is often argued to be mainly affected by the type and extent of reactive oxygen species (ROS) formation. We tested for this by adding a selective hydroxyl radical scavenger tertiary-butanol (t-BuOH) to aerobic exposures between *S. MR-1* and the three materials (Fig. S9). ATP analyses showed that *S. MR-1* viability increased slightly in nZVI systems but significantly more in $\text{Na}_2\text{S}_2\text{O}_4\text{-nZVI}$ exposures; that is, a ~ 2 -fold increase in ATP viability after 120 minutes with added t-BuOH (Fig. S9). However, in $\text{Na}_2\text{S-nZVI}$ exposures, the addition of t-BuOH led to a further decrease in ATP viability, meaning it increased toxicity. While these observations reaffirm that nZVI and $\text{Na}_2\text{S}_2\text{O}_4\text{-nZVI}$ materials behave similarly qualitatively, but differently to $\text{Na}_2\text{S-nZVI}$, it is difficult to conclude much else from these data other than ROS probably played a greater role in $\text{Na}_2\text{S}_2\text{O}_4\text{-nZVI}$ than nZVI aerobic inactivation. Indeed, it suggests that the ROS chemistry of these materials is probably quite complex, particularly considering the complexity of the surface shell chemistry of these materials and that ROS scavengers themselves may interact with particle surfaces. The

latter may be the reason for the enhanced toxicity in $\text{Na}_2\text{S-nZVI}$ exposures with added t-BuOH. Oxidative stress levels induced by aerobic exposure to nZVI and S-nZVI have only been explored for *P. putida* so far; toxicity was highest in exposures to nZVI but decreased by increasing sulfidation for $\text{Na}_2\text{S-S-nZVI}$ type materials (Semerád *et al.* 2020). However, no information on ROS speciation was derived, which may best be done in cell-free experiments (Song *et al.* 2017).

Under anaerobic conditions, toxicity is presumed to be mainly mediated by physical and/or chemical cell membrane disruption and particle penetration into cells (Cheng *et al.* 2019b; Han *et al.* 2019; Lee *et al.* 2008). ATP/CFU viabilities in nZVI, $\text{Na}_2\text{S}_2\text{O}_4\text{-nZVI}$ and $\text{Na}_2\text{S-nZVI}$ anaerobic exposures were fairly similar, although trends in nZVI and $\text{Na}_2\text{S}_2\text{O}_4\text{-nZVI}$ exposures seemed more similar to each other than to $\text{Na}_2\text{S-nZVI}$ (based on Δ_{Assay} data in Fig. 3f). To gain insight into the cell-particle association in these anaerobic exposures, SEM imaging was done on cells collected after 60-minute exposures (Fig. 4). In $\text{Na}_2\text{S-nZVI}$ exposures, cells were largely free of $\text{Na}_2\text{S-nZVI}$ particles and the particles themselves seemed intact. Conversely, in nZVI and $\text{Na}_2\text{S}_2\text{O}_4\text{-nZVI}$ exposures, cell surfaces were covered with flake-like structures and it was difficult to find intact, spherical nZVI and $\text{Na}_2\text{S}_2\text{O}_4\text{-nZVI}$ particles. Similar observations were also made in a previous nZVI toxicity study with *Bacillus subtilis* (Diao and Yao 2009). Overall, these observations suggest that nZVI and $\text{Na}_2\text{S}_2\text{O}_4\text{-nZVI}$ particles became unstable and a new, flake-like secondary phase formed, which was associated closely with the cells. It is well known that nZVI materials corrode quickly via interaction with water, which then leads to the formation of secondary Fe mineral phases such as $\text{Fe}(\text{OH})_2$ (Diao and Yao 2009; He *et al.* 2016). This seemed to be the case in nZVI and $\text{Na}_2\text{S}_2\text{O}_4\text{-nZVI}$ exposures while in the $\text{Na}_2\text{S-nZVI}$ exposure, there appears to be significantly less corrosion, probably because the FeS_m shell formed a well-defined layer around the Fe^0 core, protecting it from fast corrosion, as shown previously (Mangayayam *et al.* 2019b). Corrosion of the $\text{Na}_2\text{S}_2\text{O}_4\text{-nZVI}$ material probably occurred much more quickly due to its more heterogeneous shell structure with both FeS_m and $\text{Fe}(\text{OH})_2$, as argued previously for similar $\text{Na}_2\text{S}_2\text{O}_4\text{-nZVI}$ materials (Mangayayam *et al.* 2019a). Considering how the varied corrosion behaviour impacted cell viability, it seems harder for cells to reproduce (as in the CFU assay) when covered with mineral precipitates compared to cells free of precipitate, as has also been argued previously in nZVI toxicity studies. This process may well explain the lower CFU viabilities observed for nZVI and $\text{Na}_2\text{S}_2\text{O}_4\text{-nZVI}$ anaerobic exposures after 60 and 120 minutes compared to $\text{Na}_2\text{S-nZVI}$ exposures (Fig. 3d).

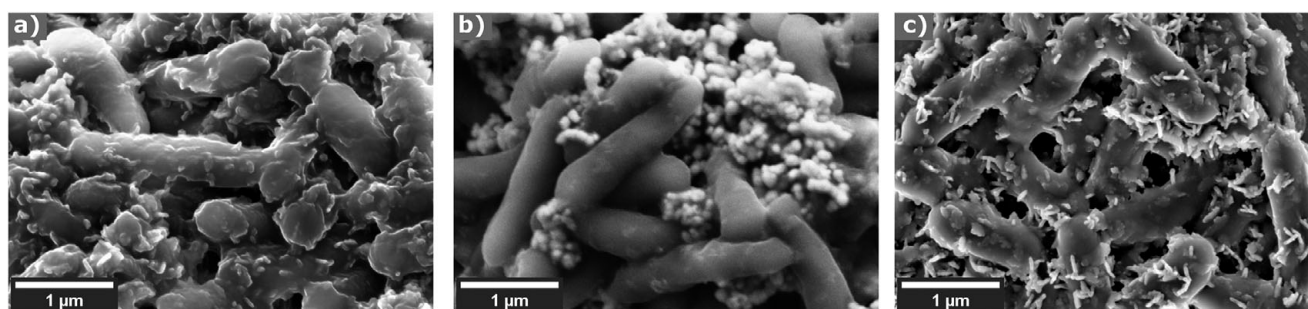


Figure 4. SEM images of *S. MR-1* after 60 minutes of anaerobic exposure to (a) nZVI with cells covered by mineral precipitates; (b) $\text{Na}_2\text{S-nZVI}$ with both cells and particles intact; (c) $\text{Na}_2\text{S}_2\text{O}_4\text{-nZVI}$ with cells covered by mineral precipitates. Note that although the SEM image gives the impression that cells and $\text{Na}_2\text{S-nZVI}$ particles form a tight aggregate, this could in part also be due to SEM sample preparation (drying effects).

The impact of cell membrane disruption and particle penetrations on *S. MR-1* viability cannot be assessed from SEM images. But, based on previous studies that performed TEM analyses, this has also been shown for $\text{Na}_2\text{S}_2\text{O}_4$ -nZVI and Na_2S type materials exposed to *E. coli* (Cheng *et al.* 2019a; Han *et al.* 2019) and, therefore, could be another toxicity pathway in the examined anaerobic systems and is possible also in aerobic exposures.

Impact of materials on the mixed KB-1[®] and field-derived culture

The viability of the KB-1[®] and in-house TCE enrichment culture was probed with the ATP assay only as the CFU method is not suitable for mixed cultures. In experiments where KB-1[®] was exposed to the three different materials at a loading of 1000 mg/L, a gradual decrease in ATP viability to 40% was observed over the first 60 hours with few differences between the tested materials (Fig. 5a). After 60 hours, trends between nZVI and S-nZVI materials started to deviate from one another. Specifically, ATP viability further decreased in the presence of nZVI, with only about 10% viability remaining after 160 hours. By contrast, in Na_2S -nZVI and $\text{Na}_2\text{S}_2\text{O}_4$ -nZVI exposures, viability stabilized around 40%. Note that trends at lower material loadings (as tested for Na_2S -nZVI, Fig. 5b) were very similar and a significant increase in

viability (roughly 35%) was only observed when the particle loading was decreased to 100 mg/L.

For comparison to KB-1[®], an in-house TCE enrichment culture was also exposed to nZVI and Na_2S -nZVI. This culture showed a much higher sensitivity to both materials compared to KB-1[®]. In the presence of nZVI, almost full inactivation (that is, complete loss of ATP-viability) of the culture was observed within the first 12 hours, while in the presence of Na_2S -nZVI, ATP-viability was reduced to about 40% after 12 hours, and practically zero after 40 hours (Fig. 5c). Similar to observations with KB-1[®], ATP viability trends of this in-house culture only changed significantly when the material loading was decreased 10-fold to 100 mg/L.

The differences in viability between these two cultures can be explained in part by differences in microbial community structure because inoculum, cultivation conditions and durations starkly differed between them. As such, they will have varied in their robustness towards exposure to these materials. Noteworthy the total ATP values in the two culture controls (no added materials, Fig. S10) remained high and comparable within the first 12 hours of the experiment (Fig. S10). Then, the viability of the in-house culture control started to decrease considerably while the viability in the KB-1 control only started to decrease after 60 hours. Reasons as to why the KB-1[®] culture strains exhibited a higher resilience towards

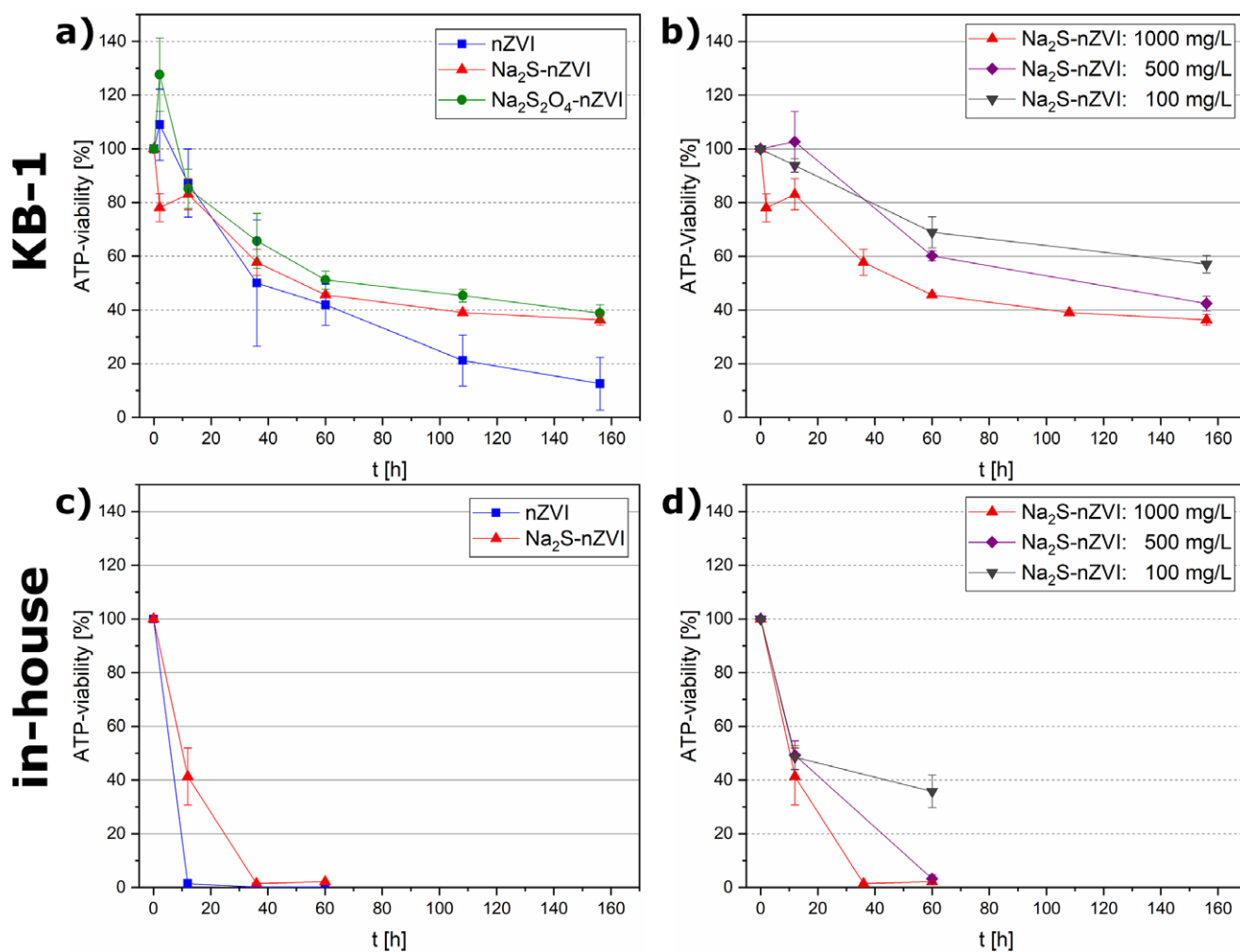


Figure 5. ATP-viability of KB-1[®] culture upon exposure to (a) the three materials at a concentration of 1000 mg/L and (b) varying concentrations of Na_2S -nZVI. ATP-viability of in-house culture upon exposure to (c) nZVI and Na_2S -nZVI at a concentration of 1000 mg/L and (d) varying concentrations of Na_2S -nZVI. Data represent averages of triplicate exposures and error bars give one standard deviation. Experiments with the in-house culture were terminated early due to low viability at high material concentrations.

the tested materials are probably rooted in the over 15 years of cultivation in the presence of reduced iron (nano) materials (precipitated from $(\text{NH}_4)_2\text{Fe}(\text{II})(\text{SO}_4)_2$ and Na_2S used as reducing agents for KB-1^o cultivation) (Edwards and Grbić-Galić 1994; Duhamel *et al.* 2002). As such, strains in the KB-1^o culture are probably better adapted to highly reducing conditions, oxidative stress by dissolved Fe^{2+} and the presence of reduced iron materials on cell surfaces. For comparison, Ti(III) nitrilotriacetic acid was used to induce sufficiently reducing conditions in the in-house cultures.

It is important to note again that the ATP assay provides only an overall (unselective) activity of the bacterial community as a whole rather than that of dechlorinating strains. A strain or process (gene) specific quantitative polymerase chain reaction (qPCR) approach may be more suitable to track the presence and/or activity of dechlorinating strains. Furthermore, spiking the mixed cultures with TCE and lactate/methanol after exposure experiments and monitoring for the evolution of biodegradation intermediates could provide further insights into the resilience of the used cultures. So far, no other study has evaluated the toxicity of nZVI and S-nZVI towards the KB-1^o culture. Summer *et al.* showed in a lysimeter experiment that nZVI can stimulate biodegradation by this culture, but no comparison between nZVI materials was made and no adverse effects were investigated or noted (Summer *et al.* 2020). Further comparison can be made with viability studies on other dechlorinating cultures. In these, the focus was on the impacts of nZVI towards the viability of *Dehalococcoides* strains, or cultures containing it, by monitoring relevant gene copies via qPCR or reductive dechlorination activity via degradation intermediates (Xiu *et al.* 2010a, 2010b; Xu *et al.* 2014; Rónavári *et al.* 2016). A strong decline in reductive dehalogenase genes within 48 hours (Xiu *et al.* 2010b) and reductive dechlorination, as well as a decrease in total *Dehalococcoides* numbers, were observed, from as low as 50–500 mg/L nZVI. High nZVI loadings (> 1000 mg/L) always led to poor recovery of the culture's dechlorination abilities unless the materials were coated with protective polymers. In particular, one study reported a 50% decrease in ATP viability when the culture was exposed to 50 mg/L nZVI for 2 hours (Velimirovic *et al.* 2015). Comparison to these studies highlights a significant resilience of KB-1^o towards nZVI and S-nZVI exposure given that, even at a high nZVI loading of 1000 mg/L, we only observed a significant decrease in ATP viability (< 80%) after 12 hours. This supports the use of the KB-1^o culture in combined abiotic–biotic treatments.

Summary and perspectives

In this study, two different S-nZVI materials were synthesized using two commonly used sulfur sources of different oxidation numbers. Sulfide (-II) treatment yielded more reduced S-nZVI shells that were chemically and physically more homogeneous and provided higher stability against anaerobic water corrosion. Dithionite (+III) yielded more oxidized S-nZVI shells that were both chemically and physically heterogeneous and left S-nZVI particles more prone to anaerobic water corrosion. Accordingly, the two S-nZVI materials exerted different degrees of toxicity towards the microbial cells tested here. In some regards, the dithionite-based S-nZVI particles showed a strong similarity to untreated nZVI, which is probably related to the more oxidized shell nature.

S. MR-1 viability upon short-term exposure to nZVI and S-nZVI materials showed that S. MR-1 viability is highest in the presence of Na_2S -nZVI, while $\text{Na}_2\text{S}_2\text{O}_4$ -nZVI and nZVI materials exhibited generally higher and similar toxicity. Furthermore, the decrease

in S. MR-1 viability was faster under aerobic compared to anaerobic conditions, independent of tested nZVI and S-nZVI materials.

In longer time frame experiments (> 60 h) with two anaerobic, reductively dechlorinating cultures, S-nZVI materials exhibited lower toxicity than nZVI. The KB-1^o culture exhibited a substantially higher tolerance towards nZVI and Na_2S -nZVI than the in-house culture or previously investigated dechlorinating cultures. This advantage is argued to stem from the presence of reduced iron solids in the KB-1^o culture medium. A significant reduction in toxicity was only observed upon a 10-fold decrease in particle loading from 1000 to 100 mg/L.

The study findings suggest that sulfidated nZVI, particularly nZVI sulfidated with Na_2S , will have an advantage over non-sulfidated nZVI in combined abiotic–biotic treatment scenarios as the inactivation of native or augmented cultures is reduced during the first week of incubation. Thus, sulfidated nZVI treatment scenarios should allow for an earlier and more rapid recovery, growth and enhanced biotic reductive dechlorination of the bacterial communities.

Supplementary material. The supplementary material for this article can be found at <https://doi.org/10.1180/gbi.2024.1>.

Acknowledgements. This research was funded by the Metal-Aid Innovative Training Network (ITN), supported by a grant from the European Commission's Marie Skłodowska Curie Actions programme under project number 675219. We would like to thank Marco Mangayayam for his help with particle synthesis; Olaf Borkiewicz, Leighanne Gallington and Kevin A. Beyer for support with X-ray total scattering measurements at beamline 11 ID-B, at Advanced Photon Source (USA); Theis Brock-Nannestad for help with GC-MS measurements and Jing Ai and Hans Christian Bruun Hansen for enabling headspace GC-FID measurements. We also thank Stanislav Jelavic, Dennis Okhrimenko and Nicolas Bovet for help with XPS measurement and Jeffrey Paolo Perez for help during SEM measurements at GFZ. Experiments at APS were supported by the U.S. Department of Energy (DOE) Office of Science User Facility, operated for the DOE Office of Science by Argonne National Laboratory under contract no. DE-AC02-06CH11357. Support for travel to APS came from the Danish Council for Independent Research (via DANSCATT).

Competing interest. There are no competing interest to declare.

References

- Atashgahi S., Häggblom M.M. and Smidt H. (2018) Organohalide respiration in pristine environments: implications for the natural halogen cycle. *Environmental Microbiology*, **20**(3), 934–948. doi:10.1111/1462-2920.14016.
- Beumer R.R., de Vries J. and Rombouts F.M. (1992) *Campylobacter jejuni* non-culturable coccoid cells. *International Journal of Food Microbiology*, **15**(1–2), 153–63. doi:10.1016/0168-1605(92)90144-R.
- Bhattacharjee S. and Ghoshal S. (2018a) Optimal design of sulfidated nanoscale zerovalent iron for enhanced trichloroethene degradation. *Environmental Science and Technology*, **52**(19), 11078–86. doi:10.1021/acs.est.8b02399.
- Bhattacharjee S. and Ghoshal S. (2018b) Sulfidation of nanoscale zerovalent iron in the presence of two organic macromolecules and its effects on trichloroethene degradation. *Environmental Science: Nano*, **5**(3), 782–91. doi:10.1039/c7en01205e.
- Chappelle E.W., Picciolo G.L. and Deming J.W. (1978) Determination of bacterial content in fluids. *Methods in Enzymology*, **57**(C), 65–72. doi:10.1016/0076-6879(78)57009-2.
- Chen J., Xiu Z., Lowry G.V. and Alvarez P.J.J. (2011) Effect of natural organic matter on toxicity and reactivity of nano-scale zero-valent iron. *Water Research*, **45**(5), 1995–2001. doi:10.1016/j.watres.2010.11.036.
- Cheng Y., Dong H., Lu Y... Zeng G. (2019a) Toxicity of sulfide-modified nanoscale zero-valent iron to *Escherichia coli* in aqueous solutions. *Chemosphere*, **220**, 523–30. doi:10.1016/j.chemosphere.2018.12.159.

- Cheng Y., Dong H., Lu Y. ... Zeng G. (2019b) Toxicity of sulfide-modified nanoscale zero-valent iron to *Escherichia coli* in aqueous solutions. *Chemosphere*, **220**, 523–30. doi:10.1016/j.chemosphere.2018.12.159.
- Diao M. and Yao M. (2009) Use of zero-valent iron nanoparticles in inactivating microbes. *Water Research*, **43**(20), 5243–5251. doi:10.1016/j.watres.2009.08.051.
- Dong H., Li L., Lu Y. ... Zeng G. (2019, March 1) Integration of nanoscale zero-valent iron and functional anaerobic bacteria for groundwater remediation: A review. *Environment International*, 265–77. doi:10.1016/j.envint.2019.01.030.
- Dong H., Xie Y., Zeng G., ... Wu Y. (2016) The dual effects of carboxymethyl cellulose on the colloidal stability and toxicity of nanoscale zero-valent iron. *Chemosphere*, **144**, 1682–89. doi:10.1016/j.chemosphere.2015.10.066.
- Duhamel M., Wehr S.D., Yu L., ... Edwards E.A. (2002) Comparison of anaerobic dechlorinating enrichment cultures maintained on tetrachloroethene, trichloroethene, cis-dichloroethene and vinyl chloride. *Water Research*, **36**(17), 4193–4202. doi:10.1016/S0043-1354(02)00151-3.
- Edwards E.A. and Grbić-Galić D. (1994) Anaerobic degradation of toluene and o-xylene by a methanogenic consortium. *Applied and Environmental Microbiology*, **60**(1), 313–22. <http://www.ncbi.nlm.nih.gov/pubmed/8117084> (accessed 21 August 2024).
- Fan D., Anitori R.P., Tebo B.M., ... Arey B.W. (2013) Reductive sequestration of pertechnetate (99TcO₄⁻) by nano zerovalent iron (nZVI) transformed by abiotic sulfide. *Environmental Science and Technology*, **47**(10), 5302–5310. doi:10.1021/es304829z.
- Fan D., Lan Y., Tratnyek P.G., ... Agrawal A. (2017) Sulfidation of iron-based materials: a review of processes and implications for water treatment and remediation. *Environmental Science and Technology*, **51**(22), 13070–85. doi:10.1021/acs.est.7b04177.
- Fan D., O'Brien Johnson G., Tratnyek P.G. and Johnson R.L. (2016) Sulfidation of nano zerovalent iron (nZVI) for improved selectivity during in-situ chemical reduction (ISCR). *Environmental Science and Technology*, **50**(17), 9558–65. doi:10.1021/acs.est.6b02170.
- Federighi M., Tholozan J.L., Cappelletti J.M., Tissier J.P. and Jouve J.L. (1998) Evidence of non-cocoid viable but non-culturable *Campylobacter jejuni* cells in microcosm water by direct viable count, CTC-DAPI double staining, and scanning electron microscopy. *Food Microbiology*, **15**(5), 539–50. doi:10.1006/fmic.1998.0181.
- García A.N., Zhang Y., Ghoshal S., He F. and O'Carroll D.M. (2021) Recent advances in sulfidated zerovalent iron for contaminant transformation. *Environmental Science & Technology*, **55**(13), 8464–83. doi:10.1021/acs.est.1c01251.
- Grosvenor A.P., Kobe B.A., Biesinger M.C. and McIntyre N.S. (2004) Investigation of multiplet splitting of Fe 2p XPS spectra and bonding in iron compounds. *Surface and Interface Analysis*, **36**(12), 1564–74. doi:10.1002/sia.1984.
- Han Y., Ghoshal S., Lowry G.V. and Chen J. (2019) A comparison of the effects of natural organic matter on sulfidated and nonsulfidated nanoscale zerovalent iron colloidal stability, toxicity, and reactivity to trichloroethylene. *Science of the Total Environment*, **671**, 254–61. doi:10.1016/j.scitotenv.2019.03.343.
- Han Y., Yang M.D.Y., Zhang W. and Yan W. (2015) Optimizing synthesis conditions of nanoscale zero-valent iron (nZVI) through aqueous reactivity assessment. *Frontiers of Environmental Science & Engineering*, **9**(5), 813–822. doi:10.1007/s11783-015-0784-z.
- He D., Ma J., Collins R.N. and Waite T.D. (2016) Effect of structural transformation of nanoparticulate zero-valent iron on generation of reactive oxygen species. *Environmental Science & Technology*, **50**(7), 3820–3828. doi:10.1021/acs.est.5b04988.
- He F. and Zhao D. (2007) Manipulating the size and dispersibility of zerovalent iron nanoparticles by use of carboxymethyl cellulose stabilizers. *Environmental Science and Technology*, **41**(17), 6216–21. doi:10.1021/es0705543.
- Kim E.J., Kim J.H., Azad A.M. and Chang Y.S. (2011) Facile synthesis and characterization of Fe/FeS nanoparticles for environmental applications. *ACS Applied Materials and Interfaces*, **3**(5), 1457–62. doi:10.1021/am200016v.
- Kim J.Y., Park H.J., Lee C., Nelson K.L., Sedlak D.L. and Yoon J. (2010) Inactivation of *Escherichia coli* by nanoparticulate zerovalent iron and ferrous ion. *Applied and Environmental Microbiology*, **76**(22), 7668–7670. doi:10.1128/AEM.01009-10.
- Kocur C.M.D., Lomheim L., Boparai H.K., ... O'Carroll D.M. (2015) Contributions of abiotic and biotic dechlorination following carboxymethyl cellulose stabilized nanoscale zero valent iron injection. *Environmental Science and Technology*, **49**(14), 8648–56. doi:10.1021/acs.est.5b00719.
- Kocur C.M.D., Lomheim L., Molenda O., ... O'Carroll D.M. (2016) Long-term field study of microbial community and dechlorinating activity following carboxymethyl cellulose-stabilized nanoscale zero-valent iron injection. *Environmental Science and Technology*, **50**(14), 7658–70. doi:10.1021/acs.est.6b01745.
- Lee C., Jee Y.K., Won I.L., Nelson K.L., Yoon J. and Sedlak D.L. (2008) Bactericidal effect of zero-valent iron nanoparticles on *Escherichia coli*. *Environmental Science and Technology*, **42**(13), 4927–4933. doi:10.1021/es800408u.
- Lefevre E., Bossa N., Wiesner M.R. and Gunsch C.K. (2015) A review of the environmental implications of in situ remediation by nanoscale zero valent iron (nZVI): Behavior, transport and impacts on microbial communities. *Science of the Total Environment*, **565**, 889–901. doi:10.1016/j.scitotenv.2016.02.003.
- Li Z., Greden K., Alvarez P.J.J., Gregory K.B. and Lowry G.V. (2010) Adsorbed polymer and NOM limits adhesion and toxicity of nano scale zerovalent iron to *E. coli*. *Environmental Science and Technology*, **44**(9), 3462–67. doi:10.1021/es9031198.
- Löffler F.E., Sanford R.A. and Ritalahti K.M. (2005) Enrichment, cultivation, and detection of reductively dechlorinating bacteria. *Methods in Enzymology*, **397**(362), 77–111. doi:10.1016/S0076-6879(05)97005-5.
- Mangayayam M., Dideriksen K., Ceccato M. and Tobler D.J. (2019a) The structure of sulfidized zero-valent iron by one-pot synthesis: impact on contaminant selectivity and long-term performance. *Environmental Science and Technology*, **53**(8), 4389–96. doi:10.1021/acs.est.8b06480.
- Mangayayam M.C., Perez J.P.H., Dideriksen K., ... Benning L.G. (2019b) Structural transformation of sulfidized zerovalent iron and its impact on long-term reactivity. *Environmental Science: Nano*, **6**(11), 3422–30. doi:10.1039/c9en00876d.
- Mullet M., Khare V. and Ruby C. (2008) XPS study of Fe(II)-Fe(III) (oxy) hydroxycarbonate green rust compounds. *Surface and Interface Analysis*, **40**(3–4), 323–28. doi:10.1002/sia.2758.
- Nurmi J.T., Sarathy V., Tratnyek P.G., Baer D.R., Amonette J.E. and Karkamkar A. (2011) Recovery of iron/iron oxide nanoparticles from solution: Comparison of methods and their effects. *Journal of Nanoparticle Research*, **13**(5), 1937–52. doi:10.1007/s11051-010-9946-x.
- Oliver J.D. (2005) The viable but nonculturable state in bacteria. *Journal of Microbiology*, **43**, 93–100.
- Oliver J.D. (2010) Recent findings on the viable but nonculturable state in pathogenic bacteria. *FEMS Microbiology Reviews*, **34**(4), 415–25. doi:10.1111/J.1574-6976.2009.00200.X.
- Pan H. and Ren Q. (2023) Wake Up! Resuscitation of viable but nonculturable bacteria: mechanism and potential application. *Food*, **12**(1), 82. doi:10.3390/FOODS12010082.
- Pérez-de-Mora A., Lacourt A., McMaster M.L., Liang X., Dworatzek S.M. and Edwards E.A. (2018) Chlorinated electron acceptor abundance drives selection of *Dehalococcoides mccartyi* (D. mccartyi) strains in dechlorinating enrichment cultures and groundwater environments. *Frontiers in Microbiology*, **9**, 812. doi:10.3389/fmicb.2018.00812.
- Rónavári A., Balázs M., Tolmacsov P., ... Kónya Z. (2016) Impact of the morphology and reactivity of nanoscale zero-valent iron (nZVI) on dechlorinating bacteria. *Water Research*, **95**, 165–73. doi:10.1016/j.watres.2016.03.019.
- Schiefler A.A., Tobler D.J., Overheu N.D. and Tuxen N. (2018) Extent of natural attenuation of chlorinated ethenes at a contaminated site in Denmark. *Energy Procedia*, **146**, 188–93. doi:10.1016/j.egypro.2018.07.024.
- Semerád J. and Cajthaml T. (2016) Ecotoxicity and environmental safety related to nano-scale zerovalent iron remediation applications. *Applied Microbiology and Biotechnology*, 9809–19. doi:10.1007/s00253-016-7901-1.
- Semerád J., Semerád J., Filip J., ... Cajthaml T. (2020) Environmental fate of sulfidated nZVI particles: The interplay of nanoparticle corrosion and toxicity during ageing. *Environmental Science: Nano*, **7**(6), 1794–1806. doi:10.1039/d0en00075b.
- Song S., Su Y., Adeleye A.S., Zhang Y. and Zhou X. (2017) Optimal design and characterization of sulfide-modified nanoscale zerovalent iron for diclofenac removal. *Applied Catalysis B: Environmental*, **201**, 211–20. doi:10.1016/j.apcatb.2016.07.055.

- Su X., Sun F., Wang Y., ... Shen C (2015) Identification, characterization and molecular analysis of the viable but nonculturable *Rhodococcus biphenylivorans*. *Scientific Reports*, **5**(1), 18590. doi:10.1038/srep18590.
- Su Y., Lowry G.V., Jassby D. and Zhang Y. (2019) Sulfide-modified NZVI (S-NZVI): Synthesis, characterization, and reactivity. Pp. 359–86 in: *Nanoscale Zerovalent Iron Particles for Environmental Restoration: From Fundamental Science to Field Scale Engineering Applications*, Cham: Springer International Publishing. doi:10.1007/978-3-319-95340-3_9.
- Summer D., Schöftner P., Wimmer B., ... Reichenauer T.G. (2020) Synergistic effects of microbial anaerobic dechlorination of perchloroethene and nano zero-valent iron (nZVI) – A lysimeter experiment. *New Biotechnology*, **57**, 34–44. doi:10.1016/j.nbt.2020.02.005.
- Sun Y.P., Li X., Cao J., Zhang W. and Wang H.P. (2006) Characterization of zero-valent iron nanoparticles. *Advances in Colloid and Interface Science*, **120** (1–3), 47–56. doi:10.1016/j.cis.2006.03.001.
- Tang J., Tang L., Feng H., ... Zhou Y. (2016) pH-dependent degradation of p-nitrophenol by sulfidated nanoscale zerovalent iron under aerobic or anoxic conditions. *Journal of Hazardous Materials*, **320**, 581–90. doi:10.1016/j.jhazmat.2016.07.042.
- Thomas P., Sekhar A.C., Upreti R., Mujawar M.M. and Pasha S.S. (2015) Optimization of single plate-serial dilution spotting (SP-SDS) with sample anchoring as an assured method for bacterial and yeast cfu enumeration and single colony isolation from diverse samples. *Biotechnology Reports*, **8**, 45–55. doi:10.1016/j.btre.2015.08.003.
- van Tatenhove-Pel R.J., Zwering E., Solopova A., Kuipers O.P. and Bachmann H. (2019) Ampicillin-treated *Lactococcus lactis* MG1363 populations contain persisters as well as viable but non-culturable cells. *Scientific Reports*, **9**(1), 1–10. doi:10.1038/s41598-019-46344-z.
- Velimirovic M., Simons Q. and Bastiaens L. (2015) Use of CAH-degrading bacteria as test-organisms for evaluating the impact of fine zerovalent iron particles on the anaerobic subsurface environment. *Chemosphere*, **134**, 338–45. doi:10.1016/j.chemosphere.2015.04.068.
- Wu D., Peng S., Yan K., Shao B., Feng Y. and Zhang Y. (2018) Enhanced As(III) sequestration using sulfide-modified nano-scale zero-valent iron with a characteristic core-shell structure: sulfidation and As distribution. *ACS Sustainable Chemistry and Engineering*, **6**(3), 3039–48. doi:10.1021/acssuschemeng.7b02787.
- Wu H., Yin J.J., Wamer W.G., Zeng M. and Lo Y.M. (2014, March 1) Reactive oxygen species-related activities of nano-iron metal and nano-iron oxides. *Journal of Food and Drug Analysis*, **22**(1), 86–94. doi:10.1016/j.jfda.2014.01.007.
- Wyckoff R.W.G. (1963) *Crystal Structures I BT - Crystal Structures Crystal Structures*, 2nd ed., New York: Interscience Publishers. Retrieved from papers3://publication/uuid/C089A728-DACD-4320-9318-E063845D17B7
- Xu Z. ming, Jin Z. hui, Li T. long, Mahendra S., Lowry G.V. and Alvarez P.J.J. (2010a) Effects of nano-scale zero-valent iron particles on a mixed culture dechlorinating trichloroethylene. *Bioresource Technology*, **101**(4), 1141–46. doi:10.1016/j.biortech.2009.09.057.
- Xu Z.M., Gregory K.B., Lowry G.V. and Alvarez P.J.J. (2010b) Effect of bare and coated nanoscale zerovalent iron on tceA and vcrA gene expression in *Dehalococcoides* spp. *Environmental Science and Technology*, **44**(19), 7647–51. doi:10.1021/es101786y.
- Xu C., Zhang B., Wang Y., ... Tratnyek P.G. (2016) Effects of sulfidation, magnetization, and oxygenation on azo dye reduction by zerovalent iron. *Environmental Science and Technology*, **50**(21), 11879–87. doi:10.1021/acs.est.6b03184.
- Xu G., Wang J. and Lu M. (2014) Complete debromination of decabromodiphenyl ether using the integration of *Dehalococcoides* sp. strain CBDB1 and zero-valent iron. *Chemosphere*, **117**(1), 455–61. doi:10.1016/j.chemosphere.2014.07.077.
- Xu J., Avellan A., Li H., ... Lowry G.V. (2020) Sulfur loading and speciation control the hydrophobicity, electron transfer, reactivity, and selectivity of sulfidized nanoscale zerovalent iron. *Advanced Materials*, **32**(17), 1906910. doi:10.1002/adma.201906910.
- Xu J., Wang Y., Weng C., ... Lowry G.V. (2019) Reactivity, selectivity, and long-term performance of sulfidized nanoscale zerovalent iron with different properties. *Environmental Science and Technology*, **53**(10), 5936–45. doi:10.1021/acs.est.9b00511.
- Zhou L., Thanh T. Le, Gong J., Kim J.H., Kim E.J. and Chang Y.S. (2014) Carboxymethyl cellulose coating decreases toxicity and oxidizing capacity of nanoscale zerovalent iron. *Chemosphere*, **104**, 155–61. doi:10.1016/j.chemosphere.2013.10.085.